Research Paper

Locally Reducing KCC2 Activity in the Hippocampus is Sufficient to Induce Temporal Lobe Epilepsy

Matt R. Kelley [a], Ross A. Cardarelli [b], Joshua L. Smalley [a], Thomas A. Ollerhead [a], Peter M. Andrew [a], Nicholas J. Brandon [b,c], Tarek Z. Deeb [a,b], Stephen J. Moss [a,b,c,d,*]

[a] Department of Neuroscience, Tufts University School of Medicine, Boston, MA, USA
[b] AstraZeneca-Tufts University Laboratory for Basic and Translational Neuroscience Research, Boston, MA, USA
[c] Neuroscience, IMED Biotech Unit, AstraZeneca, Boston, MA, USA
[d] Department of Neuroscience, Physiology and Pharmacology, University College, London, WC1E, 6BT, UK

ARTICLE INFO

ABSTRACT

Mesial temporal lobe epilepsy (mTLE) is the most common form of epilepsy, believed to arise in part from compromised GABAergic inhibition. The neuronal specific K^+/Cl^- co-transporter 2 (KCC2) is a critical determinant of the efficacy of GABAergic inhibition and deficits in its activity are observed in mTLE patients and animal models of epilepsy. To test if reductions of KCC2 activity directly contribute to the pathophysiology of mTLE, we locally ablated KCC2 expression in a subset of principal neurons within the adult hippocampus. Deletion of KCC2 resulted in compromised GABAergic inhibition and the development of spontaneous, recurrent generalized seizures. Moreover, local ablation of KCC2 activity resulted in hippocampal sclerosis, a key pathological change seen in mTLE. Collectively, our results demonstrate that local deficits in KCC2 activity within the hippocampus are sufficient to precipitate mTLE.

1. Introduction

Mesial temporal lobe epilepsy (mTLE) is the most common form of human epilepsy, classified by unprovoked, spontaneous seizures originating within the temporal lobe. mTLE in humans develops over a latent period of several years after a precipitating insult such as traumatic brain injury, hypoxia, infection, or episodes of status epilepticus [1,2]. In addition to seizures, profound morphological changes are observed in the brain, the most common being hippocampal sclerosis [3]. Sclerotic hippocampal tissue surgically removed from human mTLE patients shows widespread neuronal loss and gliosis [4]. Similar changes are seen in convulsant-induced rodent models of mTLE [5].

While the cellular mechanisms that underlie the development of mTLE remain poorly understood, deficits in the efficacy of γ-aminobutyric acid (GABA) mediated inhibitory neurotransmission are widely believed to be of significance [6–8]. Fast synaptic inhibitory transmission in the brain is primarily mediated by chloride (Cl^-)-permeable γ-aminobutyric acid receptors ($GABA_ARs$), which upon opening hyperpolarize the cell membrane through Cl^- influx and decrease neuronal firing. During development, the electroneutral

K^+/Cl^- co-transporter 2 (KCC2) becomes the dominant mediator of Cl^- extrusion, coupling Cl^- efflux to the outwardly directed K^+ gradient [9,10]. Deficits in KCC2-mediated Cl^- extrusion result in increased intracellular Cl^- levels, permitting depolarizing $GABA_AR$ responses [11]. KCC2 loss-of-function mutations in human patients result in severe cases of epilepsy in infancy with migrating focal seizures [12,13]. In mice, a global loss of 95% of KCC2 results in seizures and mortality at 2–3 weeks postnatal [14], and loss-of-function mutations increase seizure susceptibility [15,16].

Reduced KCC2 levels and depolarizing $GABA_AR$ signaling are observed in tissue surgically removed from mTLE patients [17–20]. In rodent models of mTLE, reduced KCC2 is observed in the hippocampus immediately after an initial precipitating injury and during subsequent epileptogenesis [21–25]. However, it is unknown if these deficits directly contribute to the development of seizures and accompanying pathophysiology of mTLE.

To test this, we have ablated KCC2 expression in a subset of principal neurons in the hippocampus of adult mice. We show that reducing KCC2 activity leads to increased neuronal Cl^- accumulation and gross deficits in GABAergic inhibition. Moreover, these deficits are sufficient to initiate recurring generalized seizures, reactive astrogliosis, and neuronal loss within the hippocampus, reproducing the core features of mTLE with hippocampal sclerosis. Thus, local inhibition of KCC2 within the hippocampus is sufficient to precipitate mTLE.

* Corresponding author at: Department of Neuroscience, Tufts University School of Medicine, Boston, MA, USA.
E-mail address: Stephen.Moss@Tufts.edu (S.J. Moss).

2. Materials and Methods

2.1. Animal Care

Animal studies were performed with protocols approved by the Institutional Animal Care and Use Committee of Tufts Medical Center. Mice were kept on a 12-h light/dark cycle with *ad libitum* access to food and water.

2.2. Generation and Genotyping of KCC2^{FL} Mice

KCC2^{FL} mice (*Slc12a5$^{lox/lox}$*) were have been described previous and have been backcrossed on the C57BL/6 J mice for 10 generations [26]. PCR was with an expected product size of 426 bp for wild-type and 543 bp for KCC2^{FL} mice.

2.3. Viral Injections

Adult (6–8 week old) male KCC2^{FL} mice were stereotaxically injected with adeno-associated virus (AAV) containing *Cre* recombinase. Prior to surgery, mice were injected with buprenorphine (0.75 mg/kg, s.c.) and anesthetized with isoflurane (1–3%). Drill holes were made above each dorsal hippocampus (coordinates: AP -2.0 mm from bregma, ML +/− 1.8 mm) and a Neuros syringe (Hamilton, Reno, NV) lowered to 2.0 mm below the brain surface. Mice were bilaterally injected with 0.5 μL of either AAV9·CaMKII·HI.eGFP-*Cre*.WPRE. SV40 or AAV9·CaMKII0.4.eGFP·WPRE.rBG (titer: 1×10^{13} GC/mL in PBS, University of Pennsylvania Vector Core, Philadelphia, PA) at a rate of 50 nL/min. After injection, the needle remained in the brain 5 min before being withdrawn. The skin was closed and mice placed on a heating pad until mobile. Mice were singly housed post-surgery.

2.4. EEG/EMG and Video Recordings

A subset of virus-injected mice were implanted with electroencephalography/electromyography (EEG/EMG) headstages (2-channel, Pinnacle Technology, Lawrence, KA) following virus injection. Implants were aligned with lambda and 4 screws inserted for subdural recording contacts above the right frontal and parietal lobes. The implant was glued to the skull and mice recovered as above. After a recovery period of 7 days, continuous paired video and EEG/EMG recordings were collected using Sirenia Acquisition software (Pinnacle). Recordings were processed using Sirenia Seizure (Pinnacle) and EEG seizure events detected using DClamp (Massachusetts General Hospital Pediatric Epilepsy Research Lab, Boston, MA). Seizure FFT spectra were created using MATLAB (Mathworks, Natick, MA).

2.5. Slice Immunohistochemistry

Mouse brains were fixed by transcardial perfusion of PBS-buffered 4% paraformaldehyde (PFA) (Electron Microscopy Services, Hatfield, PA) and removed to 4% PFA overnight, then cryoprotected in 30% sucrose solution in PBS for 3 days before being frozen in optimal cutting temperature medium (VWR, Radnor, PA). 40 μm serial coronal sections were prepared using a Leica SM-2000R microtome (Wetzlar, Germany). Sections were kept at −20°C in cryoprotectant solution (876 mM sucrose, 4 M polyvinylpyrrolidone, 30% ethylene glycol, and 10% PBS in diH$_2$O), and washed with PBS before blocking. Sections were blocked with 10% normal goat serum (NGS) and 0.3% Triton X-100 in PBS for 2 h at room temperature. Sections were incubated overnight with either anti-KCC2 C-terminus (1:500 rabbit, Millipore 07–432, Darmstadt, Germany), anti-GFAP (1:5000 mouse, Millipore MAB360), or anti-NeuN (1:1000 mouse, Millipore MAB377). Slices were subsequently labeled with Alexa-Fluor secondary antibodies (1:200; Thermo Fisher Scientific, Waltham, MA) prior to mounting with ProLong Gold with or without DAPI (Thermo Fisher). To measure KCC2 expression levels

Z-stack images were taken of the hippocampus at 20× using an Eclipse Ti confocal microscope (Nikon, Tokyo, Japan). Regions of interest (ROI) were drawn in the CA1 or DG and the average intensity for each ROI was normalized to the maximum average intensity per animal. Slices of each animal were averaged and compared between groups at equivalent time-points after virus injection. For NeuN, images were taken at 60× of CA1 principal layer or dentate gyrus granule cell layer, and 100 μm^2 ROIs drawn. NeuN positive labeled cells were counted in each ROI, averaged for each animal and compared between groups. For GFAP labeling, images were obtained using a scanning fluorescence microscope (BZ-X700, Keyence, Osaka, Japan) at 10x magnification. ROIs were drawn around the CA1 or DG in each slice. A threshold was used create a binary mask of GFAP labeling, and area calculated for ROI and reported as amount of GFAP labeling/mm^2. Values from each animal were averaged and then compared between groups. All image processing was performed using FIJI (ImageJ).

2.6. Slice Electrophysiology

Mice were anesthetized with isofluorane and brains removed. Coronal slices (350 μm) were cut on a Leica VT1000s vibratome in ice-cold cutting solution containing (in mM): 87 NaCl, 2.5 KCl, 0.5 CaCl$_2$, 25 NaHCO$_3$, 1.25 NaH$_2$PO$_4$, 7 MgCl$_2$, 50 sucrose and 25 glucose, pH 7.4. Slices were placed in a submerged chamber for a 1 h recovery period at 32 °C in artificial cerebrospinal fluid (aCSF) containing (in mM): 126 NaCl, 26 NaHCO$_3$, 2.5 KCl, 2 MgCl$_2$, 2 CaCl$_2$, 1 glutamine, 1.25 NaH$_2$PO$_4$, 1.5 Na-pyruvate and 10 glucose. All solutions were bubbled with 95% O$_2$/5% CO$_2$. *Gramicidin Perforated Patch Recordings.* After a 1-h recovery, slices were placed in a submerged chamber (RC-27 L, Warner Instruments, Hamden, CT). For perforated patch, micropipettes (3–4 MΩ) contained saline (in mM): 140 KCl and 10 HEPES, pH 7.4 KOH, and were backfilled with gramicidin D (50 μg/mL, Sigma Aldrich) to establish access resistances between 20 and 80 MΩ throughout the recording period. Dentate gyrus granule cells were patched in the outer 2/3 of the granule cell layer to avoid newborn granule cells. A glass pipette (1–3 MΩ tip resistance) filled with muscimol (10 μM, Tocris Bioscience, Bristol, UK) in aCSF was lowered into the molecular layer of the dentate gyrus and pulses (500 ms) applied locally by pressure ejection with a Picospritzer II (General Valve, Fairfield, NJ) to activate GABA$_A$-mediated currents in granule cells held at voltages between −100 to −50 mV in 10-mV increments. E$_{GABA}$ values were obtained from linear regression fits to the data at voltages near the observable reversal potential of I$_{muscimol}$. Tetrodotoxin (TTX, 400 nM, Tocris) was applied to block activity-dependent shifts in E$_{GABA}$ and bumetanide (10 μM, Tocris) to inhibit NKCC1, and VU0463271 to inhibit KCC2 (1 μM, AstraZeneca, Cambridge, UK). Voltages were corrected offline with a liquid junction potential value of 3.8 mV. Recordings were performed with a Multiclamp 700B amplifier and Clampex 10 acquisition software. Data were low-pass filtered at 10 kHz and analyzed offline with Clampfit (Molecular Devices, Sunnyvale, CA).

2.7. Primary Neuron Culture

Primary cortical/hippocampal neurons were prepared and cultured as previously described [27]. Briefly, P0 KCC2^{FL} mice were anesthetized on ice and the brains removed. The brains were dissected in Hank's buffered salt solution (HBSS, Invitrogen) with 10 mM HEPES. The cortices and hippocampi were tripsinized and triturated to dissociate the neurons. Cells were counted using a hemocytometer and plated on poly-L-lysine-coated coverslips (for ICC and electrophysiology) or in 35 mm dishes (for immunoblot) at a density of 1×10^5 or 4×10^5 cells respectively. At days *in vitro* (DIV) 18, cells were exposed to control or *Cre* AAV as described above at a concentration of 1×10^6 GC/mL. To determine effect on neuronal viability, GFP-positive cells were counted at DIV 24.

2.8. Immunocytochemistry

Immunocytochemistry (ICC) was carried out as previously described [28]. Briefly, primary cultured neurons were washed with PBS, fixed in 4% PFA in PBS, and permeabilized with 0.1% Triton X-100 in PBS. The cells were then blocked in a solution containing 5% BSA and 5% goat serum. Primary and secondary antibodies (as described above) were prepared at a dilution of 1:1000 in block solution and incubated with the cells for 1 h at room temperature in the dark. The cells were washed in PBS and mounted using ProLong Gold.

2.9. Immunoblotting

Immunoblotting was carried out as previously described [29]. Briefly, proteins were isolated in RIPA lysis buffer (50 mM Tris, 150 mM NaCl, 0.1% SDS, 0.5% sodium deoxycholate and 1% Triton X-100, pH 7.4) and quantified using a Bradford assay (Bio-Rad, Hercules, CA, USA). Samples were prepared in sample buffer and 20 μg of protein was loaded onto a 7% (for KCC2) or 10% (for α-tubulin) polyacrylamide gel. Proteins were separated by sodium dodecyl sulfate poly-acrylamide gel electrophoresis (SDS-PAGE) and transferred onto nitrocellulose membrane. Membranes were blocked in 5% milk in tris-buffered saline 1% Tween-20 (TBS-T) and incubated with primary antibodies anti-KCC2 C-terminus (1:1000 rabbit, Millipore 07-432), anti-KCC2 N-terminus (1:1000 rabbit, LS-C135150, LifeSpan Biosciences, Seattle, WA) or α-tubulin (1:5000 mouse, Sigma-Aldrich) for 1 h. The membranes were washed and incubated for 1 h at room temperature with HRP-conjugated secondary antibodies (1:5000 – Jackson ImmunoResearch Laboratories, West Grove, PA, USA). Protein bands were visualized with Pierce ECL (ThermoFisher) and imaged using a ChemiDoc MP (Bio-Rad).

2.10. Culture Electrophysiology

Neurons were recorded at 33 °C in saline containing (in mM) 140 NaCl, 2.5 KCl, 2.5 MgCl$_2$, 2.5 CaCl$_2$, 10 HEPES, 11 glucose, pH 7.4 (NaOH). All solutions were applied through a three-barrel microperfusion apparatus (700 μm, Warner Instruments, Hampden, CT), and conducted in the presence of tetrodotoxin (300 nM) and bumetanide (10 μM) to block voltage-dependent sodium channels and NKCC1, respectively. Cells infected with control- or Cre-containing virus were selected by epifluorescence for GFP expression. Data were acquired using Clampex 10 software at an acquisition rate of 10 kHz with an Axopatch 2B amplifier and digitized with a Digidata 1440 (Molecular Devices). To detect endogenous Cl$^-$ levels, cells were perforated with gramicidin (50 mg/mL) dissolved in an internal pipette containing (in mM) 140 KCl, 10 HEPES, pH 7.4 (KOH) and a tip resistance of 3–4 MΩ. Following perforation to below a series resistance of 100 MΩ, E$_{GABA}$ values were found by application of muscimol (1 μM) during positive-going voltage ramps (20 mV/s).

2.11. Statistical Analysis

Statistical analysis was performed with GraphPad 7 (San Diego, CA) and R. Unpaired Student's t-tests were used unless otherwise indicated. Data were expressed as mean ± SEM, with significance set at α = 0.05.

3. Results

3.1. Deletion of KCC2 in Cultured Hippocampal Neurons Increases Neuronal Cl- Levels and Compromises GABAergic Inhibition

We have recently developed mice in which KCC2 expression can be inactivated via Cre-recombinase mediated excision of exons 22-25 in the respective gene SCN12A5. The deleted regions encodes the C-terminal amino acids 911-1096 (KCC2^{FL} Fig. 1A). These residues have been established to play an essential role in transporter activity [30,31].

To assess the efficacy of this approach cultured neurons from the KCC2^{FL} mice were infected with adeno-associated viruses expressing fluorescent GFP and Cre recombinase under the control of the CaMKIIα promoter (AAV9-CaMKII-eGFP-Cre; AAV-Cre) to restrict expression of the respective transgene to principal neurons [32]. 18-DIV hippocampal cultures prepared from KCC2^{FL} homozygotes were infected with AAV-Cre or a similar virus construct containing GFP (AAV9-CaMKII-eGFP; AAV-GFP) and 3–6 days later detergent solubilized lysates were subjected to immunoblotting with antibodies that recognize the C or N-
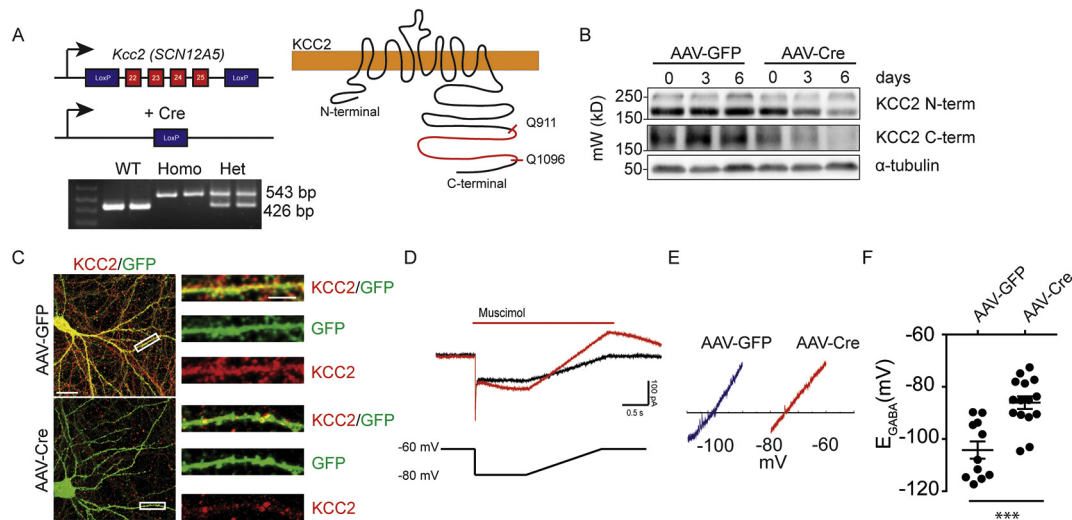

Fig. 1. Conditional inactivation of KCC2 in cultured neurons leads to elevated intracellular Cl$^-$ levels. A. KCC2^{FL} mice were generated with LoxP sites flanking exons 22–25. PCR products from mice showing discrimination between wild type, homozygous, or heterozygous for KCC2^{FL} gene. Upon Cre expression, LoxP recombination resulted in deletion of the C-terminal portion of the transporter between residues Q911-Q1096. B. Neuronal cultures from KCC2^{FL} mice were treated with either control AAV9-CaMKII-eGFP (AAV-GFP) or AAV9-CaMKII-eGFP-Cre (AAV-Cre) and the lysates probed with antibodies directed against N-terminal and C-terminal epitopes on KCC2. Both N- and C-terminal portions of the KCC2 protein were reduced in AAV-Cre treated cultures with increasing durations after infection. C. The efficacy of Cre-mediated knockout was confirmed using ICC on virus treated cultures using the C-terminal antibody. F. Muscimol-activated currents (red trace) and membrane leak currents (black trace) were recorded during voltage ramps in gramicidin perforated patch recordings. The voltage ramp protocol is shown below the traces and is aligned temporally. E. Exemplar leak-subtracted muscimol-activated currents from AAV-GFP and AAV-Cre neurons. The estimated E$_{GABA}$ value is where the traces cross the X-axis. F. Basal E$_{GABA}$ values were shifted to more positive levels in Cre-positive cultured neurons compared to controls. (***p < 0.001).

terminus of KCC2. Consistent with recombination, immunoreactivity of the C-terminal antibody, which recognizes epitopes within 911–1096, was dramatically reduced in neurons infected with AAV-*Cre* but not those infected with AAV-GFP. Parallel reductions in immunoreactivity were also seen with an antibody that recognizes the N-terminus of KCC2 (Fig. 1B). Immunocytochemistry labeling confirmed the reduction of KCC2 (Fig. 1C) Thus, deletion of residues 911-1096 leads to reduced steady state accumulation of KCC2.

To assess if the *Cre*-induced deficits in KCC2 expression impact chloride homeostasis, we performed gramicidin perforated patch recordings on cultured neurons 4 days after AAV infection. We measured E_{GABA} by calculating the reversal potential of leak-subtracted muscimol (1 μM; a GABA$_A$R agonist) currents during positive-directed voltage ramps. To isolate the role of KCC2 in setting E_{GABA}, we performed these recordings in the presence of the NKCC1 inhibitor bumetanide (10 μM) and blocked neuronal activity with TTX (500 nM) to prevent activity-dependent Cl$^-$ accumulation. KCC2^{FL} neurons infected with AAV-*Cre* had a positive shift in E_{GABA} compared with those infected with AAV-GFP (Fig. 1D–F; AAV-GFP = -104 ± 3 mV, $n = 11$, AAV-*Cre* = -86 ± 2 mV, $p < 0.001$, $n = 15$). Collectively these studies in culture suggest that deletion of residues 911–1096 within KCC2 decreases KCC2 expression levels, and elevated levels of intracellular Cl$^-$.
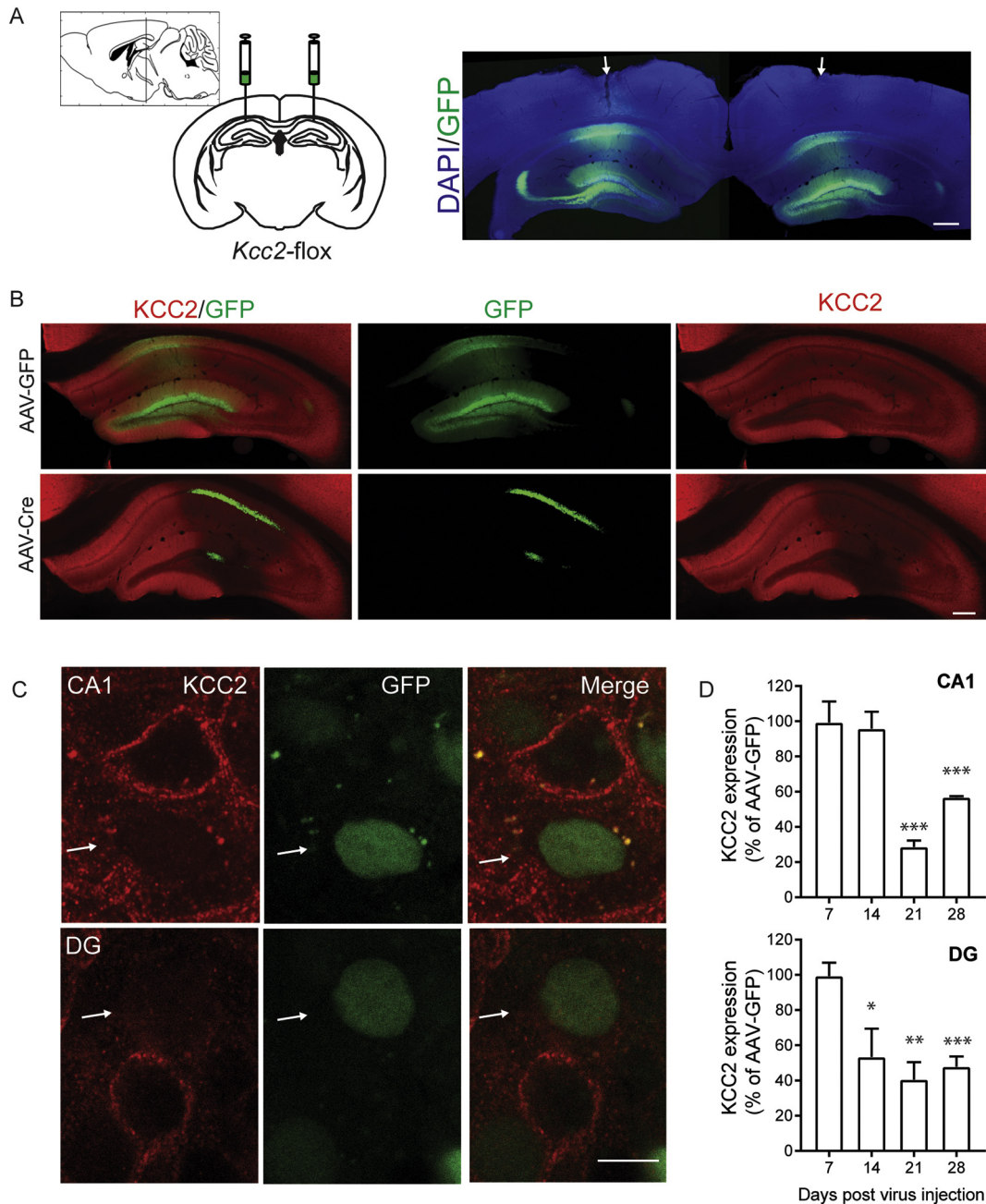

Fig. 2. Reducing KCC2 *in vivo* in subset of principal neurons in the hippocampus. A. Adult KCC2^{FL} male mice were injected bilaterally into the dorsal hippocampus with either AAV9-CaMKII-eGFP-*Cre* (AAV-*Cre*) or AAV9-CaMKII-eGFP (AAV-GFP). Arrows mark site of injection. (Scale bar = 200 μm). B. Immunohistochemical labeling of KCC2 and GFP expression in the dorsal hippocampus of mice 21 days after virus injection (Scale bar = 100 μm). C. 100× image taken from AAV-*Cre* mice at 21 days post injection, demonstrating GFP positive neurons in the CA1 principal cell layer and granule cells in the dentate gyrus with lack of KCC2 labeling (white arrows, Scale bar = 10 μm). D. Quantification of immunofluorescence in the CA1 and dentate gyrus demonstrated a significant decrease of KCC2 in AAV-*Cre* injected mice (*$p < 0.05$, **$p < 0.005$, *** $p < 0.0005$).

3.2. Viral Infection Results in Local Deficits of KCC2 Expression in the Hippocampus of KCC2^{FL} Mice

To test the significance of our *in vitro* measurements, AAV-*Cre* or AAV-GFP were bilaterally injected into the hippocampus of 6–8 wk. old KCC2^{FL} mice (Fig. 2A). The effects of viral infection on KCC2 expression levels was then examined 7–28 days after injection using immunohistochemistry coupled with confocal microscopy.

GFP expression was evident in the hippocampus of KCC2^{FL} mice injected with either virus with robust endogenous fluorescence being seen in the CA1 and dentate gyrus (DG; Fig. 2A, B). 100× Z-stack images taken at 21 days post showed loss KCC2 in GFP positive neurons, from mice infected with AAV-*Cre* (Fig. 2C). In the AAV-*Cre* injected mice, GFP positive neurons with deficits in KCC2 expression were found adjacent to non-infected neurons which exhibited high levels of KCC2 staining. To provide quantitative information on expression levels, KCC2 immunoreactivity was measured in defined regions of interest (ROI) within CA1 and dentate gyrus (DG) of mice 7, 14, 21 or 28 days post virus. Steady state accumulation of KCC2 was observed significantly reduced in both CA1 and DG in AAV-*Cre* compared with AAV-GFP using an antibody recognizing an epitope within the C-terminus (Measured as percent of AAV-GFP controls, CA1: 7-day: $99.4 \pm 11.9\%$ $p = 0.9597$, 14-day: $95.8 \pm 9.7\%$ $p = 0.6827$, 21-day: $28.6 \pm 3.6\%$ $p < 0.0001$, 28-day: $56.8 \pm 0.7\%$ $p < 0.0001$, AAV-*Cre* DG: 7-day: $99.3 \pm 7.7\%$ $p = 0.933$, 14-day: $53.4 \pm 16.1\%$ $p = 0.044$, 21-day: $40.6 \pm 9.9\%$ $p = 0.0038$, 28-day: $47.8 \pm 5.9\%$ $p = 0.0009$). Thus, our viral strategy results in focal and specific deficits in KCC2 expression levels within the hippocampus.

3.3. Reducing KCC2 Expression in the Hippocampus Leads to Elevations in Neuronal Cl- Levels and Deficits in GABAergic Inhibition

To assess the effects of reducing KCC2 expression on GABA$_A$R signaling, we prepared acute hippocampal slices from mice 14–17 days after virus infection. Perforated patch clamp recordings were performed on dentate gyrus granule cells (DGGCs) which exhibited GFP fluorescence. A puffer pipette containing muscimol (10 μM) was placed in the molecular layer to elicit GABA$_A$R mediated currents (Fig. 3A). The NKCC1 inhibitor bumetanide was applied to inhibit the contribution of NKCC1 and the voltage-gated sodium channel inhibitor TTX to block activity dependent shifts in Cl$^-$. Steady state GABA$_A$R-mediated currents were then measured at several holding potentials and this data used to determine E$_{GABA}$. DGGCs infected with AAV-*Cre* showed more positive E$_{GABA}$ values compared to those infected with AAV-GFP (Fig. 3B; AAV-GFP $= -94 \pm 3$ mV, AAV-*Cre* $= -59 \pm 7$ mV, $p = 0.002$, n = 6). In $I = 0$ recordings, 5 of 6 AAV-*Cre* infected DGGCs exhibited depolarizing membrane potential responses to muscimol, while only 1 of 6 AAV-GFP infected DGGCs showed a depolarizing response. Subtracting V$_M$ from E$_{GABA}$ values showed that AAV-*Cre* infection flipped the GABA$_A$R driving force (DF$_{GABA}$) from negative to positive values (Fig. 3C; DF$_{GABA}$AAV-GFP $= -12 \pm 4$ mV, DF$_{GABA}$AAV-*Cre* $= 18 \pm 10$ mV, $p = 0.021$, n = 6).

To further analyze Cl$^-$ extrusion, we assessed the effects of the KCC2 inhibitor VU0463271 (1 μM) on E$_{GABA}$ over a 15 min time course for DGGCs held at -70 mV [11,33]. In DGGCs infected with AAV-GFP, muscimol-activated currents became progressively smaller but were unaffected in those infected with AAV-*Cre* (Fig. 3D). E$_{GABA}$ was then determined at 15 min of treatment with VU0463271 infected neurons (AAV-GFP $= -69 \pm 5$ mV, AAV-*Cre* $= -57 \pm 4$ mV $n = 5$-6, $p = 0.1025$). ΔE$_{GABA}$ was found as the difference between pre and post VU0463271 E$_{GABA}$ values. This parameter exhibited a significant positive shift in AAV-GFP compared to those infected with AAV-*Cre* (Fig. 3E; AAV-GFP $= 25 \pm 6$ mV, AAV-*Cre* $= 2 \pm 4$ mV, p = 0.010, n = 5-6). Finally, there was no difference in resting membrane potential between the two groups (AAV-GFP $= -83 \pm 5$ mV; AAV-*Cre* $= -82 \pm 8$ mV, $p = 0.914$, n = 6). Thus, reducing KCC2 expression levels in the dentate gyrus leads to increased neuronal Cl$^-$ accumulation and the appearance of depolarizing GABA$_A$R currents, hallmarks of compromised GABAergic inhibition.

3.4. KCC2^{FL} Mice Infected with AAV-Cre Develop Spontaneous Seizures

To assess the significance of reducing KCC2 activity on the development of epilepsy, KCC2^{FL} mice were subject to continuous EEG/EMG and video recording for up to 21 days after injection of AAVs. 2-channel EEG recordings were processed using DClamp Software, and generalized
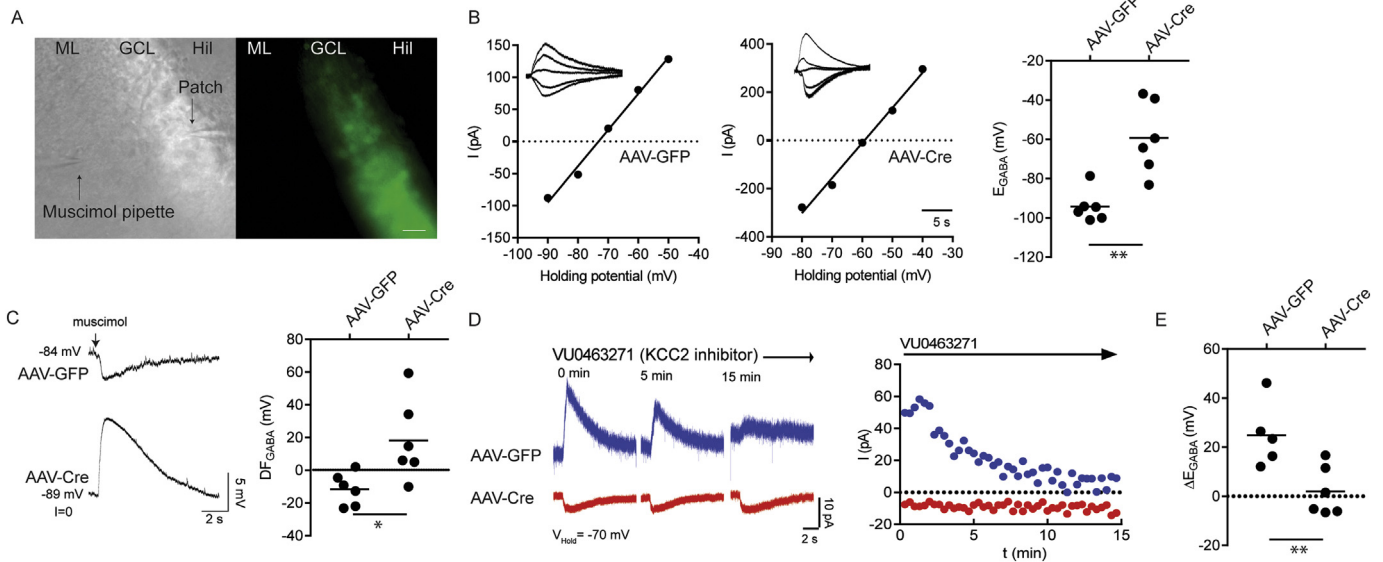

Fig. 3. Conditional deletion of KCC2 in mature dentate granule cells results in a shift in E$_{GABA}$. Dentate granule cells were patched in acute coronal slices prepared from KCC2^{FL} mice injected with either AAV-*Cre* or AAV-GFP. A. Infected neurons were identified by GFP fluorescence and targeted for gramicidin perforated patch recordings (ML = molecular layer, GCL = granule cell layer, Hil = Hilus, Scale bar = 30 μm). B. Muscimol pulses were applied at different membrane holding potentials to determine E$_{GABA}$. AAV-*Cre* granule cells showed a positive shift in E$_{GABA}$ compared to those infected with AAV-GFP. C. Muscimol (10 μM, 500 ms) pulses established the direction of GABA$_A$R signaling while holding the cell in $I = 0$. AAV-*Cre* granule cells showed a positive shift in the driving force of GABA$_A$ mediated currents compared to AAV-GFP. D. Slices were treated with the KCC2 inhibitor VU0463271 (1 μM, 15 min) and the amplitude of muscimol currents was measured periodically every 20s at holding potential of -70 mV. Example traces from AAV-GFP and AAV-*Cre* dentate granule cells. E. The difference between between E$_{GABA}$ measurements obtained before and after the VU0463271 was calculated. AAV-*Cre* granule cells displayed loss of E$_{GABA}$ sensitivity to VU0463271 (*$p < 0.05$, **$p < 0.005$).
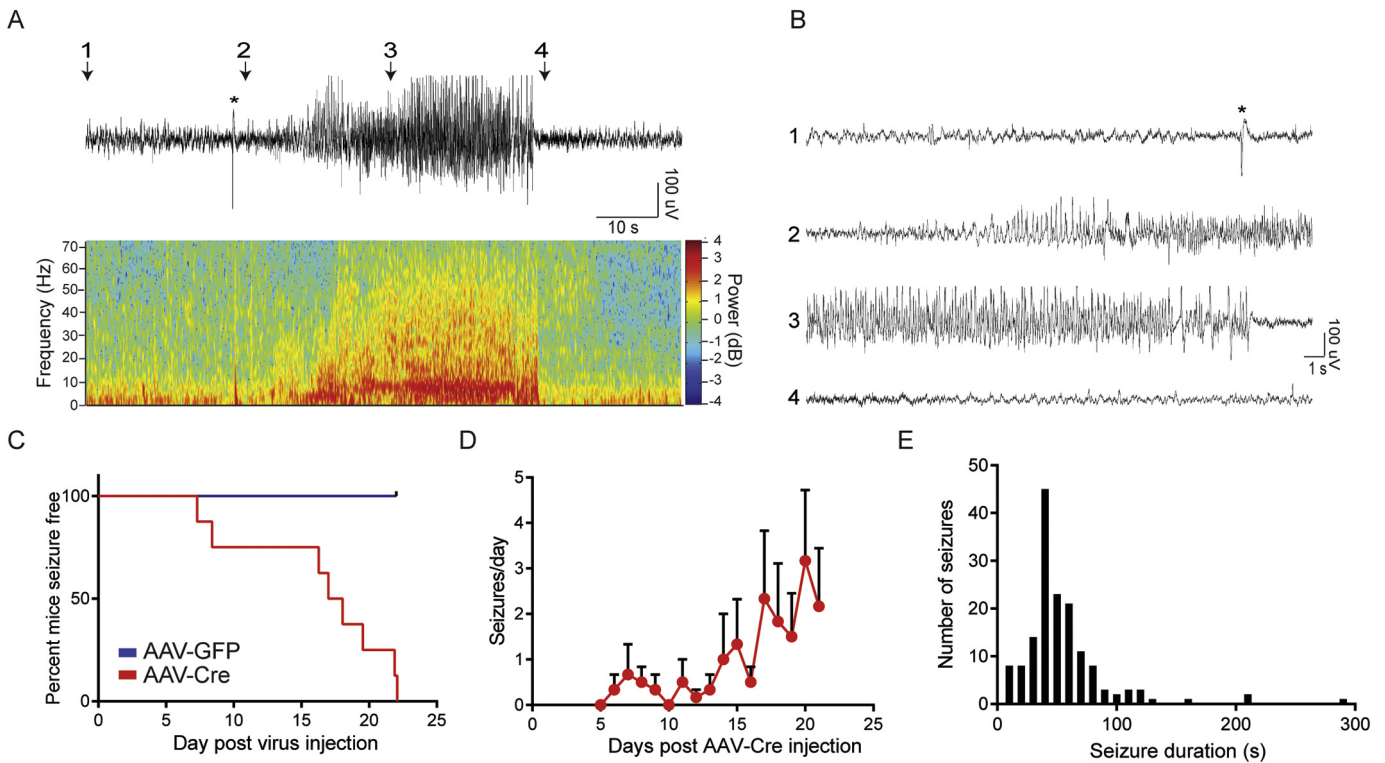
Fig. 4. Reducing KCC2 in the adult hippocampus results in generalized seizure activity. A. Continuous EEG/EMG paired video recordings were performed from KCC2^{FL} mice injected with either AAV-*Cre* or AAV-GFP into the dorsal hippocampus. Example seizure from an AAV-*Cre* injected KCC2^{FL} mouse along with wavelet spectrogram demonstrating frequency power content of the signal. B. Zoomed traces of seizure event shown in A. C. All AAV-*Cre* infected mice demonstrated generalized seizures, while no seizures were observed in AAV-GFP mice ($n = 8$ each group). D. Seizure frequency in AAV-*Cre* group in days post virus injection. E. The mean seizure duration from AAV-*Cre* group was 54.4 ± 2.9 s ($n = 154$ seizures).

seizure events detected in recordings from AAV-*Cre* injected group. These generalized seizures were characterized by increased EEG power and behavioral tonic-clonic seizures (Fig. 4A and Supplementary Videos 1 and 2). All mice infected with AAV-*Cre* developed generalized seizures while no seizures were evident in those infected with AAV-GFP ($n = 8$ mice per treatment). The mean onset of generalized seizures was 16.3 ± 3.0 days following injection of AAV-*Cre* (Fig. 4C, $n = 154$ seizures). At 21-days post AAV-*Cre* injection, KCC2^{FL} mice had a mean 2 ± 1 generalized seizures per day (Fig. 4D). Seizure events had a mean duration of 54.4 ± 2.9 s (Fig. 4E). Thus, focally reducing KCC2 expression in the hippocampus is sufficient to induce spontaneous, generalized seizures.

3.5. KCC2^{FL} Mice Infected With AAV-Cre Develop Gliosis and Neuronal Loss

In addition to spontaneous seizures, mTLE is characterized by profound hippocampal changes which include increased gliosis and decreased neuronal number [3,34]. Therefore, we assessed if reducing KCC2 activity in the hippocampus has any effects on these parameters. We first stained brain sections from infected mice with antibodies against glial fibrillary acidic protein (GFAP), the expression of which is dramatically increased in reactive astrocytes [35]. Slices visualized using confocal microscopy and low power images revealed a dramatic increase in GFAP immunoreactivity in the hippocampus of mice injected with AAV-*Cre* but not those with AAV-GFP (Fig. 5A). To provide quantitative information we compared GFAP immunoreactivity in CA1 or DG of mice 21 days after infection. Increased GFAP staining was evident in the CA1 of mice infected with AAV-Cre relative to AAV-GFP (Fig. 5C; AAV-GFP = $17,750 \pm 7192$ GFAP+ pixels/mm^2, AAV-*Cre* = $149,777 \pm 40,908$ GFAP+ pixels/mm^2, $n = 3$ mice, $p = 0.0336$). Similar increase in GFAP levels were seen in the DG; (Fig. 5D; AAV-GFP = $17,728 \pm 6962$ GFAP+ pixels/mm^2, $n = 3$ mice, AAV-*Cre* = $115,547 \pm 28,819$ GFAP+ pixels/mm^2, $n = 3$ mice, $p = 0.030$).

To examine possible effects on neuronal number, sections were stained with antibodies against NeuN, a neuronal specific protein. The number of NeuN positive cells was then determined in GFP positive ROIs within the CA1 and DG regions. 21 days after infection there was a significant decrease in the number of NeuN positive cells in CA1 of mice infected with AAV-*Cre* compared to AAV-GFP (Fig. 6; AAV-GFP = 109 ± 4 cells/100 μm^2, AAV-*Cre*: 78 ± 6 cells/100 μm^2, $p = 0.011$, $n = 3$ mice). In contrast, the number of NeuN positive structures was comparable in the DG granule cell layer (Fig. 6C; AAV-GFP = 140 ± 4 cells/100 μm^2, AAV-*Cre* = 135 ± 11 cells/100 μm^2, $p = 0.750$, $n = 3$ mice).

To further explore the relationship between KCC2 activity and neuronal viability we assessed the effects of reducing KCC2 expression in neuronal culture. To do so, cultured neurons from KCC2^{FL} mice were infected with AAV-*Cre* or AAV-GFP at 18 Div. The number of GFP positive cells was then compared 6 days later. The number of GFP expressing neurons was significantly reduced in cultures infected with AAV-*Cre* compared to AAV-GFP (Fig. 7 AAV-GFP: 17 ± 1 neurons/frame, AAV-*Cre*: 8 ± 1 neurons/frame, $p < 0.0001$, $n = 12$ frames taken from 3 coverslips for each virus treatment). Thus, KCC2 expression *per-se* appears to be a determinant of mature neuronal viability in this reduced preparation.

Collectively these results suggest that in addition to precipitating spontaneous seizures, decreasing KCC2 levels in the hippocampus leads to gliosis throughout the hippocampus and neuronal loss in CA1. Moreover, our studies in neuronal culture suggest that decreasing KCC2 is sufficient to decrease neuronal viability.

4. Discussion

The mechanisms that underlie the development of mesial temporal lobe epilepsy (mTLE) are poorly understood. It is generally accepted that deficits in the efficacy of GABAergic inhibition are of significance
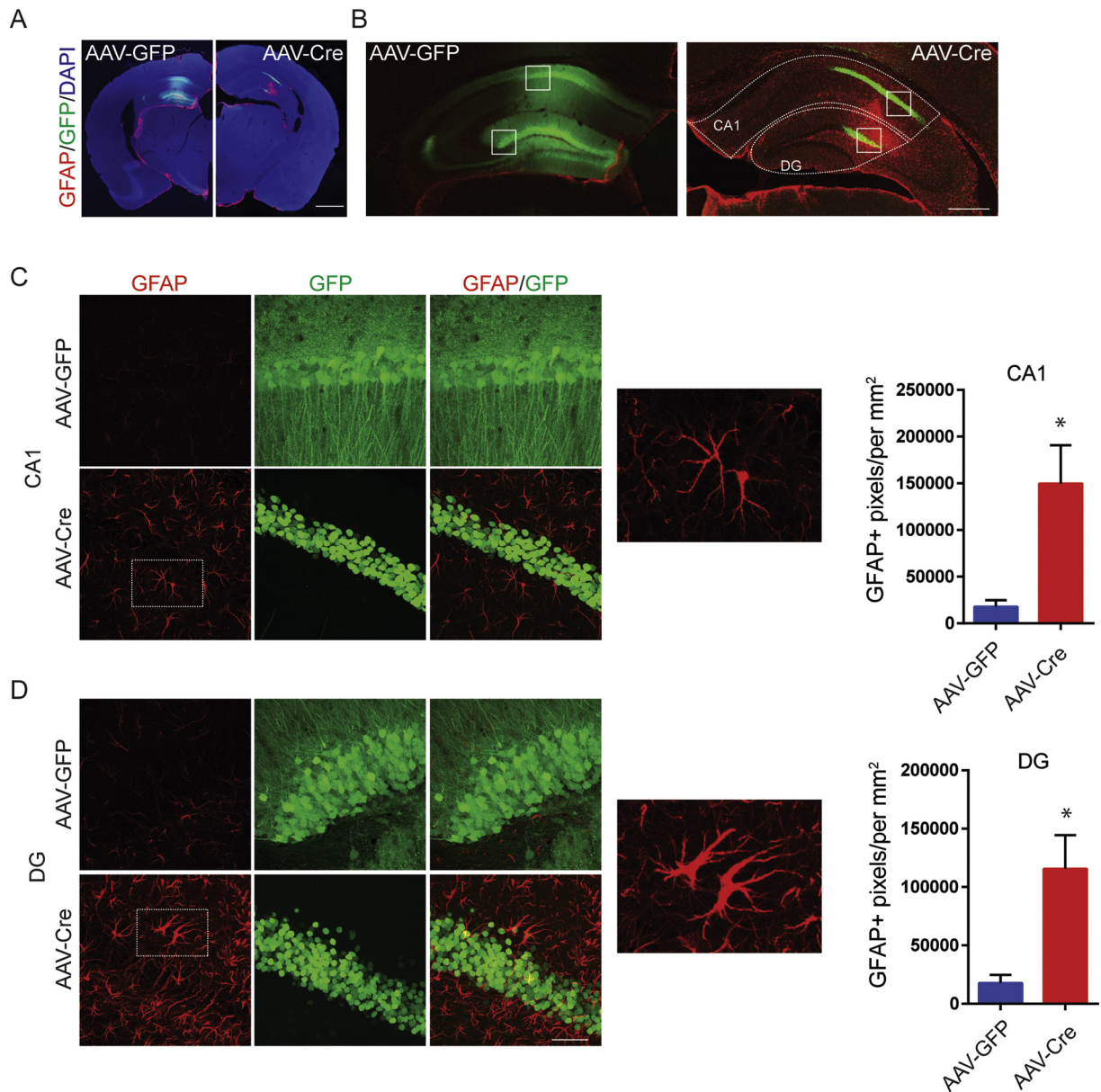
Fig. 5. Reducing KCC2 locally in hippocampus results in the development of reactive astrogliosis. A. KCC2^{FL} mice were injected with either AAV-*Cre*, or AAV-GFP. Coronal slices prepared 21 days post-viral injection were labeled for GFAP, a marker of reactive gliosis (Scale bar = 200 μm). B. Image of the dorsal hippocampus of KCC2^{FL} mice infected with AAV-*Cre*, or AAV-GFP. Region of interest (dashed lines) were drawn around complete CA1 or DG (Scale bar = 200 μm) and images quantified using binary threshold for GFAP. C. Expanded images from B (white boxes) of CA1 pyramidal layer. Mice infected with AAV-*Cre*, mice showed an increase in GFAP-labeled area and reactive astroglia. D. Expanded images from B (white boxes) of DG granule cell layer. Mice infected with AAV-*Cre*, showed an increase in GFAP-labeled area and reactive astroglia in GFP positive areas (*p < 0.05, Scale bar = 50 μm).

[7]. Fast synaptic inhibition is critically dependent upon neuronal hyperpolarization caused by Cl$^-$ influx, and accordingly deficits in KCC2 are seen in humans and animal models of epilepsy. Here we have addressed if focally reducing KCC2 in adult mouse hippocampus directly contributes to the development of the underlying pathophysiology of mTLE. Using stereotaxic injection, we locally infected the hippocampus of KCC2^{FL} mice with AAV virus expressing *Cre* under the control of the CaMKIIα promoter, facilitating specific recombination and KCC2 deletion in pyramidal neurons [32]. To validate our approach, we first infected cultured hippocampal neurons from KCC2^{FL} mice and showed through immunoblotting that 18 DIV *Cre*-expressing neurons displayed gross decreases in the expression levels of KCC2 compared to *Cre*-negative controls. In parallel, gramicidin perforated patch experiments demonstrated that E$_{GABA}$ was positively shifted reflecting increased Cl$^-$ accumulation. Our results suggest that deletion of the C-terminus of native expressed KCC2 leads to its degradation, and parallel deficits in KCC2 activity.

To assess if our studies in culture translated to similar events in the brain, we introduced AAVs into the hippocampus of 6–8-week-old KCC2^{FL} mice using stereotaxic injection. We then examined viral infection using immunofluorescence up to several weeks after infection. GFP expression was evident within the hippocampus shortly after injection. The expression levels of KCC2 were then compared between GFP-*Cre* and GFP-*Cre*-negative control injected mice. Time dependent reductions in KCC2 expression were only evident in GFP-Cre expressing mice and seen in both CA1 and the DG. In keeping with these reductions in KCC2 expression, significant positive shifts in E$_{GABA}$ were recorded in GFP-*Cre* but not GFP-*Cre*-negative DG cells 14–17 days post virus injection. Furthermore, these E$_{GABA}$ shifts resulted in a switch from hyperpolarizing to depolarizing GABA$_A$R currents. The role that KCC2 activity plays in regulating neuronal Cl- accumulation in the brain has recently been questioned by a recent publication suggesting that neuronal Cl- levels are determined by impermeant anions within the extracellular
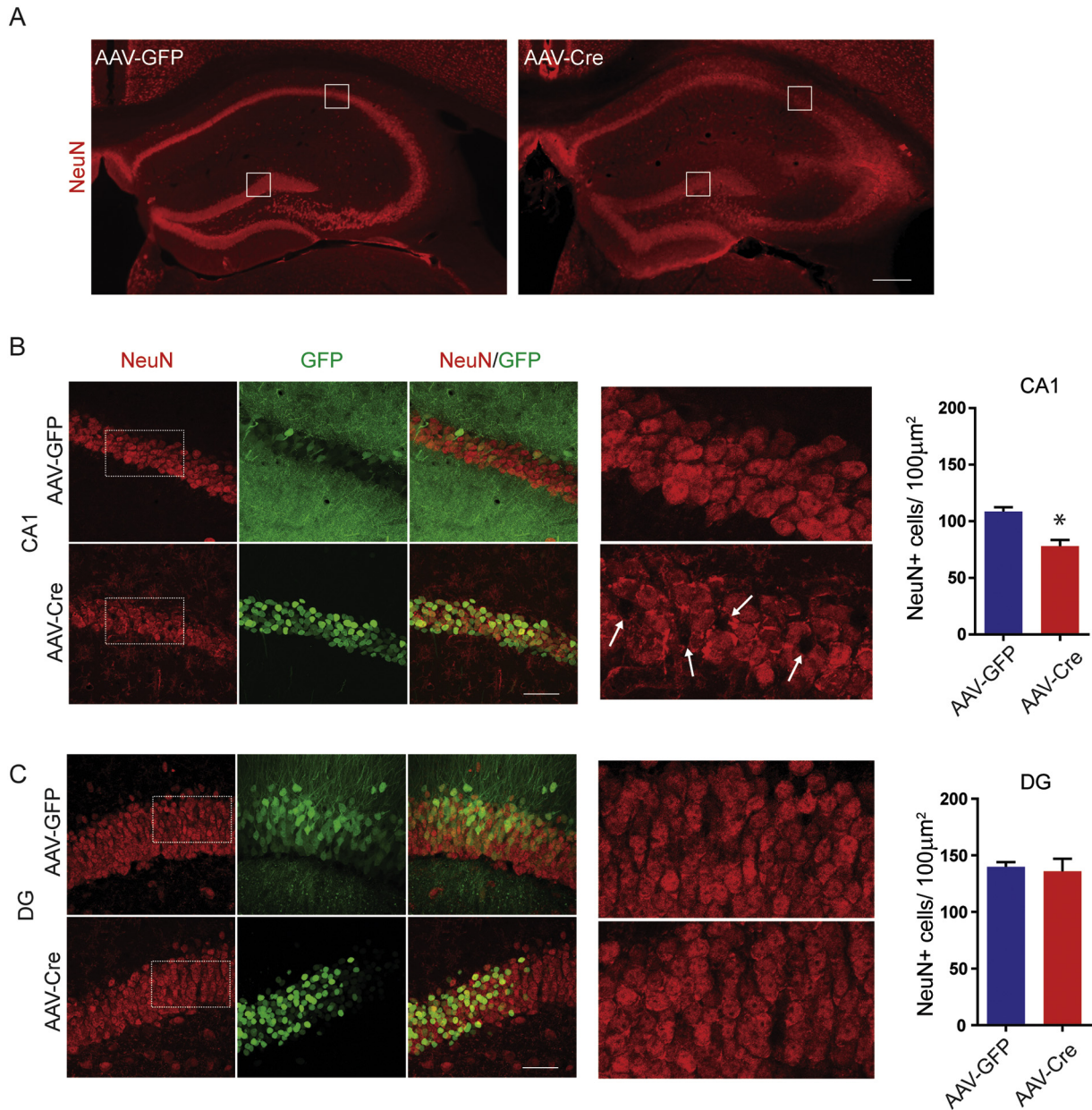
Fig. 6. Reducing KCC2 locally in hippocampus results in neuronal loss in CA1. A. KCC2^{FL} mice were injected with either AAV-*Cre* or AAV-GFP. Coronal slices prepared 21 days post-viral injection were labeled for NeuN, a neuronal marker. Region of interests of 100 μm^2 were drawn in area CA1 pyramidal layer or DG granule cell layer. White boxes are magnified in B and C (Scale bar = 200 μm). B. NeuN positive cells were counted in GFP positive regions of CA1 pyramidal layer (Scale bar = 50 μm). Arrows in expanded images of NeuN labeling indicate sites of neuronal loss. There was a reduction in NeuN positive cells within the CA1 pyramidal layer in AAV-*Cre* mice (*$p < 0.05$). C. NeuN positive cells were counted in GFP-positive regions of DG granule cell layer. No significant difference in cell count was observed.

matrix [36]. However, our results strongly suggest that KCC2 activity is critical in setting E$_{GABA}$ and the efficacy of fast GABAergic inhibition in cultured hippocampal neurons and in acute brain slices.

Computational modeling has suggested that reducing the efficacy of KCC2 mediated Cl$^-$ transport in a subset of pyramidal neurons increases the probability of seizure-like events [37]. To directly test this hypothesis *in vivo*, we performed continuous paired EEG and video recordings on KCC2^{FL} mice with induced focal deficits in KCC2 in the hippocampus. All mice infected with GFP-*Cre* developed spontaneous, generalized seizures that recurred sporadically over the entire duration of our recordings. We observed no seizures in mice infected with GFP-*Cre*-negative. Thus, our results suggest that compromising KCC2 expression within subset of pyramidal neurons in the hippocampus is sufficient to induce epilepsy. Consistent with our results, deficits in KCC2 activity have been widely reported in convulsant-induced animal models of epilepsy in

rodents prior to the onset of generalized seizures [21,23], and in brain tissue surgically removed from refractory mTLE patients [17–20]. Our results support that deficits in KCC2 activity within pyramidal neurons of mature neuronal networks is a likely contributing factor to the initiation of epileptiform activity.

Central to the progression and pathophysiology of mTLE is the observation of hippocampal sclerosis (HS), which is reproduced in animal models [34,38,39]. Thus, we assessed in parallel with the appearance of spontaneous seizures if focal deletion of KCC2 in the hippocampus leads to sclerosis. Significantly, the critical hallmarks of sclerosis—reduced neuronal number and enhanced gliosis—were seen in the hippocampus of KCC2^{FL} mice expressing GFP-*Cre* but not GFP alone. It is interesting to note that deletion of KCC2 appeared to selectively induce neuronal loss in CA1 compared to the DG. Similar preferential losses of CA1 neurons are seen in humans with mTLE [41], but the underlying mechanisms
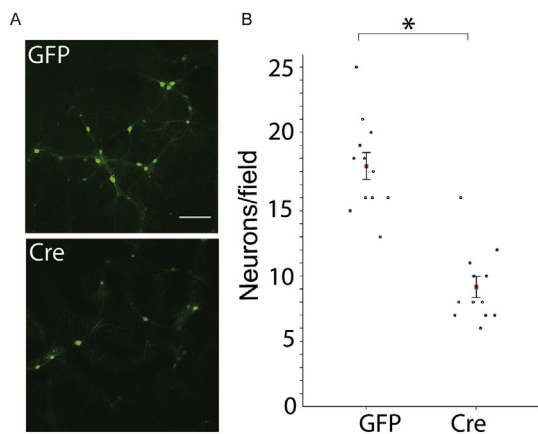
A

B

Fig. 7. Reducing KCC2 decreases neuronal viability *in vitro*. A. Neuronal cultures from KCC2^{FL} mice were treated with either control AAV9-CaMKII-eGFP (GFP) or AAV9-CaMKII-eGFP-*Cre* (*Cre*) at DIV 18 and GFP positive cells counted at DIV 24. B. There was a cell-loss of GFP positive cells in AAV-*Cre* treated cultures (*$p < 0.001$).

of the increased susceptibility of this region to neuronal loss remain to be explored. Consistent with our experiments in whole animals, *Cre*-mediated deletion of KCC2 was sufficient to reduce neuronal viability of cultured KCC2^{FL} neurons. These findings support a former study that showed that decreasing KCC2 levels in mature neuronal culture using shRNA decreases neuronal viability [42]. Our results are the first experiment *in vivo* to show that ablating KCC2 in subsets of neurons results in decreased neuronal viability.

In summary, our results suggest that locally compromising KCC2 activity within the hippocampus is sufficient to reproduce the core physiological and anatomical deficits associated with mesial temporal lobe epilepsy with hippocampal sclerosis, including spontaneous, recurring seizures, neuronal loss and gliosis. Thus, agents that potentiate KCC2 activity may be useful in treating mTLE.

Supplementary data to this article can be found online at https://doi.org/10.1016/j.ebiom.2018.05.029.

Funding Sources

Declaration of Interests

SJM serves as a consultant for SAGE Therapeutics and AstraZeneca, relationships that are regulated by Tufts University.

Author Contributions

Conceptualization and Methodology, S.J.M, N.J.B., M.R.K., T.Z.D., Investigation, M.R.K, R.A.C., J.L.S., T.A.O., P.M.A., Writing, M.R.K., J.L.S., T.Z.D, R.A.C., S.J.M, N.J.B Resources, S.J.M., N.J.B. Funding acquisition S.J.M., T.Z.D., M.R.K, N.J.B. Supervision, S.J.M.

Research in Context

Mesial temporal lobe epilepsy (mTLE) is the most common form of human epilepsy and arises largely due to deficits in the strength of inhibitory neurotransmission, a process that is in part dependent upon the neuron specific K$^+$/Cl$^-$ co-transporter KCC2. To directly test the role KCC2 plays in mTLE we have used genetic manipulation to reduce its activity in subsets of neurons in the mouse hippocampus.

Reducing KCC2 activity compromised neuronal inhibition and was sufficient to precipitate mTLE. Collectively these results suggest that deficits in KCC2 activity directly contribute to the development of mTLE. Thus, agents that elevate KCC2 activity may be useful treatments for mTLE.

References

[1] Engel J. Introduction to temporal lobe epilepsy. Epilepsy Res 1996;26:141–50.
[2] Engel J. Mesial temporal lobe epilepsy: what have we learned? Neuroscientist 2001;7(4):340–52. https://doi.org/10.1177/107385840100700410.
[3] Wieser H-G. ILAE commission report. Mesial temporal lobe epilepsy with hippocampal sclerosis. Epilepsia 2004;45(6):695–714.
[4] De Lanerolle NC, Lee TS, Spencer DD. Histopathology of human epilepsy. In: Noebels JL, Avoli M, Rogawski MA, et al, editors. Jasper's basic mechanisms of the epilepsies. 4th ed. Bethesda (MD): National Center for Biotechnology Information (US); 2012.
[5] Buckmaster PS, Dudek FE. Neuron loss, granule cell axon reorganization, and functional changes in the dentate gyrus of epileptic kainate-treated rats. J Comp Neurol 1997;385(3):385–404.
[6] Treiman DM. GABAergic mechanisms in epilepsy. Epilepsia 2001;42(Suppl. 3):8–12.
[7] Miles R, Blaesse P, Huberfeld G, Wittner L, Kaila K. Chloride homeostasis and GABA signaling in temporal lobe epilepsy. In: Noebels JL, Avoli M, Rogawski MA, et al, editors. Jasper's basic mechanisms of the epilepsies. 4th ed. Bethesda (MD): National Center for Biotechnology Information (US); 2012.
[8] Kaila K, Ruusuvuori E, Seja P, Voipio J, Puskarjov M. GABA actions and ionic plasticity in epilepsy. Curr Opin Neurobiol 2014;26:34–41.
[9] Rivera C, Voipio J, Payne JA. The K+/Cl- co-transporter KCC2 renders GABA hyperpolarizing during neuronal maturation. Nature 1999;397:251–5.
[10] Payne JA, Stevenson TJ, Donaldson LF. Molecular characterization of a putative K-cl cotransporter in rat brain. J Biol Chem 1996;271:16245–52.
[11] Sivakumaran S, Cardarelli R, Maguire J, Kelley MR, Silayeva L, Morrow DH, et al. Selective inhibition of KCC2 leads to hyperexcitability and epileptiform discharges in hippocampal slices and in vivo. J Neurosci 2015;35:8291–6.
[12] Saitsu H, Watanabe M, Akita T, Ohba C, Sugai K. Impaired neuronal KCC2 function by biallelic SLC12A5 mutations in migrating focal seizures and severe developmental delay. Sci Rep 2016 (July):1–5.
[13] Stödberg T, McTague A, Ruiz AJ, Hirata H, Zhen J, Long P, et al. Mutations in SLC12A5 in epilepsy of infancy with migrating focal seizures. Nat Commun 2015;6:8038.
[14] Woo N-S, Lu J, England R, McClellan R, Dufour S, Mount DB, et al. Hyperexcitability and epilepsy associated with disruption of the mouse neuronal-specific K-cl cotransporter gene. Hippocampus 2002;12(2):258–68.
[15] Silayeva L, Deeb TZ, Hines RM, Kelley MR, Munoz MB, Lee HHC, et al. KCC2 activity is critical in limiting the onset and severity of status epilepticus. Proc Natl Acad Sci U S A 2015;112(11):3523–8.
[16] Chen L, Wan L, Wu Z, Ren W, Huang Y, Qian B, et al. KCC2 downregulation facilitates epileptic seizures. Sci Rep 2017;7(1):156.
[17] Cohen I, Navarro V. On the origin of Interictal activity in human temporal lobe epilepsy in vitro. Science 2002;298(November):1418–22.
[18] Huberfeld G, Wittner L, Clemenceau S, Baulac M, Kaila K, Miles R, et al. Perturbed chloride homeostasis and GABAergic signaling in human temporal lobe epilepsy. J Neurosci 2007;27(37):9866–73.
[19] Muñoz A, Méndez P, DeFelipe J, Alvarez-Leefmans FJ. Cation-chloride cotransporters and GABA-ergic innervation in the human epileptic hippocampus. Epilepsia 2007;48(4):663–73.
[20] Palma E, Amici M, Sobrero F, Spinelli G, Di Angelantonio S, Ragozzino D, et al. Anomalous levels of cl⁻ transporters in the hippocampal subiculum from temporal lobe epilepsy patients make GABA excitatory. Proc Natl Acad Sci 2006;103(22):8465–8.
[21] Barmashenko G, Hefft S, Aertsen A, Kirschstein T, Kohling R. Positive shifts of the GABAA receptor reversal potential due to altered chloride homeostasis is widespread after status epilepticus. Epilepsia 2011;52(9):1570–8.
[22] Bragin DE, Sanderson JL, Peterson S, Connor JA, Müller WS. Development of epileptiform excitability in the deep entorhinal cortex after status epilepticus. Eur J Neurosci 2009;30(4):611–24.
[23] Pathak HR, Weissinger F, Terunuma M, Carlson GC, Hsu F-C, Moss SJ, et al. Disrupted dentate granule cell chloride regulation enhances synaptic excitability during development of temporal lobe epilepsy. J Neurosci 2007;27(51):14012–22.
[24] Yu J, Proddutur A, Elgammal FS, Ito T, Santhakumar V. Status epilepticus enhances tonic GABA currents and depolarizes GABA reversal potential in dentate fast-spiking basket cells. J Neurophysiol 2013;109(7):1746–63.
[25] Li X, Zhou J, Chen Z, Chen S, Zhu F, Zhou L. Long-term expressional changes of Na+-K+-Cl- co-transporter 1 (NKCC1) and K+-cl- co-transporter 2 (KCC2) in CA1 region of hippocampus following lithium-pilocarpine induced status epilepticus (PISE). Brain Res 2008;1221:141–6.
[26] Melón LC, Hooper A, Yang X, Moss SJ, Maguire J. Inability to suppress the stress-induced activation of the HPA axis during the peripartum period engenders deficits in postpartum behaviors in mice. Psychoneuroendocrinology 2017;90:182–93.
[27] Terunuma M, Vargas KJ, Wilkins ME, Ramírez OA, Jaureguiberry-Bravo M, Pangalos MN, et al. Prolonged activation of NMDA receptors promotes dephosphorylation and alters postendocytic sorting of GABAB receptors. Proc Natl Acad Sci U S A 2010;107(31):13918–23.
[28] Nakamura Y, Morrow DH, Modgil A, Huyghe D, Deeb TZ, Lumb MJ, et al. Proteomic characterization of inhibitory synapses using a novel phluorin-tagged γ-aminobutyric acid receptor, type a (GABAA), α2 subunit knock-in mouse. J Biol Chem 2016;291(23):12394–407.

[29] Varadarajan S, Bampton ETW, Smalley JL, Tanaka K, Caves RE, Butterworth M, et al. A novel cellular stress response characterised by a rapid reorganisation of membranes of the endoplasmic reticulum. Cell Death Differ 2012;19(12):1896–907.

[30] Mercado A, Broumand V, Zandi-Nejad K, Enck AH, Mount DB. A C-terminal domain in KCC2 confers constitutive K+-Cl - cotransport. J Biol Chem 2006;281(2):1016–26.

[31] Acton BA, Mahadevan V, Mercado A, Uvarov P, Ding Y, Pressey J, et al. Hyperpolarizing GABAergic transmission requires the KCC2 C-terminal ISO domain. J Neurosci 2012;32(25):8746–51.

[32] Wang X, Zhang C, Szábo G, Sun QQ. Distribution of CaMKIIα expression in the brain in vivo, studied by CaMKIIα-GFP mice. Brain Res 2013;1518:9–25.

[33] Delpire E, Baranczak A, Waterson AG, Kim K, Kett N, Morrison RD, et al. Further optimization of the K-Cl cotransporter KCC2 antagonist ML077: development of a highly selective and more potent in vitro probe. Bioorg Med Chem Lett 2012;22 (14):4532–5.

[34] Calderon-Garcidueñas AL, Mathon B, Lévy P, Bertrand A, Mokhtari K, Samson S, et al. New clinicopathological associations and histoprognostic markers in ILAE types of hippocampal sclerosis. Brain Pathol 2018. https://doi.org/10.1111/bpa.12596.

[35] Pekny M, Nilsson M. Astrocyte activation and reactive gliosis. Glia 2005;50(4): 427–34.

[36] Glykys J, Dzhala V, Egawa K, Balena T, Saponjian Y, Kuchibhotla KV, et al. Local impermeant anions establish the neuronal chloride concentration. Science 2014; 343(6171):670–5.

[37] Buchin A, Chizhov A, Huberfeld G, Miles R, Gutkin BS. Reduced efficacy of the KCC2 cotransporter promotes epileptic oscillations in a subiculum network model. J Neurosci 2016;36(46):11619–33.

[38] Borges K, Gearing M, McDermott DL, Smith AB, Almonte AG, Wainer BH, et al. Neuronal and glial pathological changes during epileptogenesis in the mouse pilocarpine model. Exp Neurol 2003;182(1):21–34.

[39] Do Nascimento AL, Dos Santos NF, Campos Pelágio F, Aparecida Teixeira S, De Moraes Ferrari EA, Langone F. Neuronal degeneration and gliosis time-course in the mouse hippocampal formation after pilocarpine-induced status epilepticus. Brain Res 2012;1470:98–110.

[41] Thom M, Sisodiya SM, Beckett A, Martinian L, Lin WR, Harkness W, et al. Cytoarchitectural abnormalities in hippocampal sclerosis. J Neuropathol Exp Neurol 2002;61(6):510–9.

[42] Pellegrino C, Gubkina O, Schaefer M, Becq H, Ludwig A, Mukhtarov M, et al. Knocking down of the KCC2 in rat hippocampal neurons increases intracellular chloride concentration and compromises neuronal survival. J Physiol 2011;589(10):2475–96.